Supporting Information - Regulating Silanol in MFI zeolites Toward Anti-coking Catalyst Rational Design for Methane Dehydroaromatization

Lihong Wei[a,*], Chuizhi Meng[a], Yuewen Sun[b], Yanlong Li[a], Rundong Li[a] and Shuai Chen[c]

[a] College of Energy and Environment, Shenyang Aerospace University, Shenyang 110136, Liaoning, China.

[b] China Nuclear Industry 23 Construction Co., Ltd, Beijing 101300 Beijing, China.

[c] State Key Laboratory of Coal Conversion, Analytical Instrumentation Center, Institute of Coal Chemistry, Chinese Academy of Science, Taiyuan, 030001, China.

*Correspondence to: weilihong@sau.edu.cn

Supporting Text

1. Different types of silanol defect structures

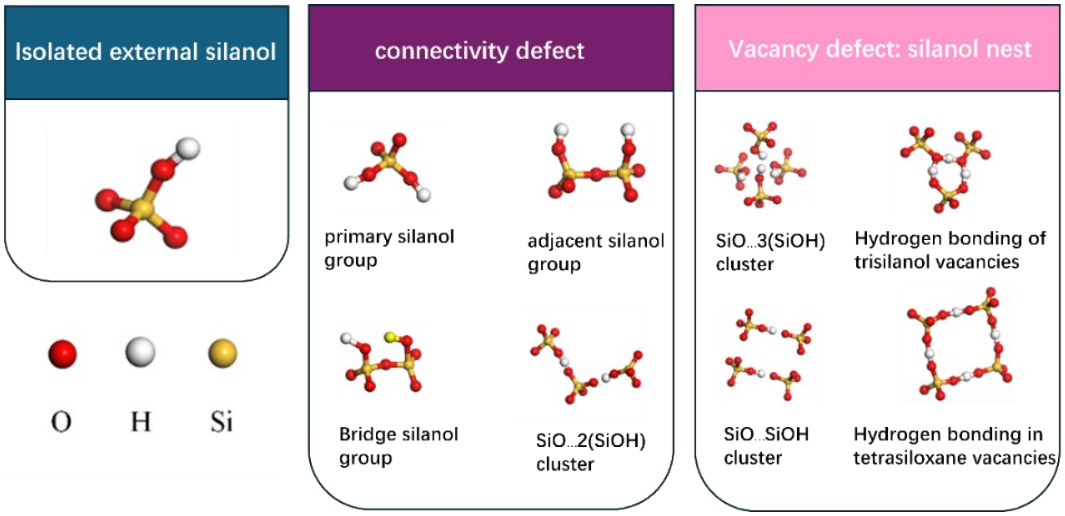

Figure S1 Schematic diagram of silanol defect structure

2. XRD patterns for MFI zeolite.

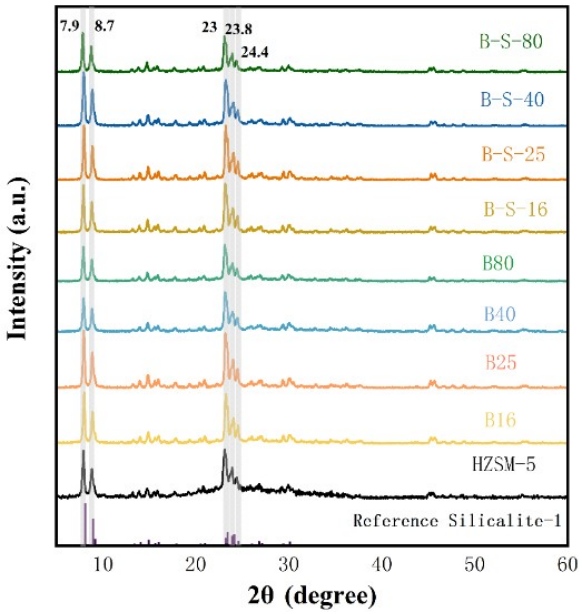

Figure S2 XRD patterns of B series samples

3. Conduct blank test without catalyst and catalytic conversion experiments on single-layer Bsn-S-X (X = 16, 25) and 3MoZ/BX double-layer catalyst methane conversion experiment.

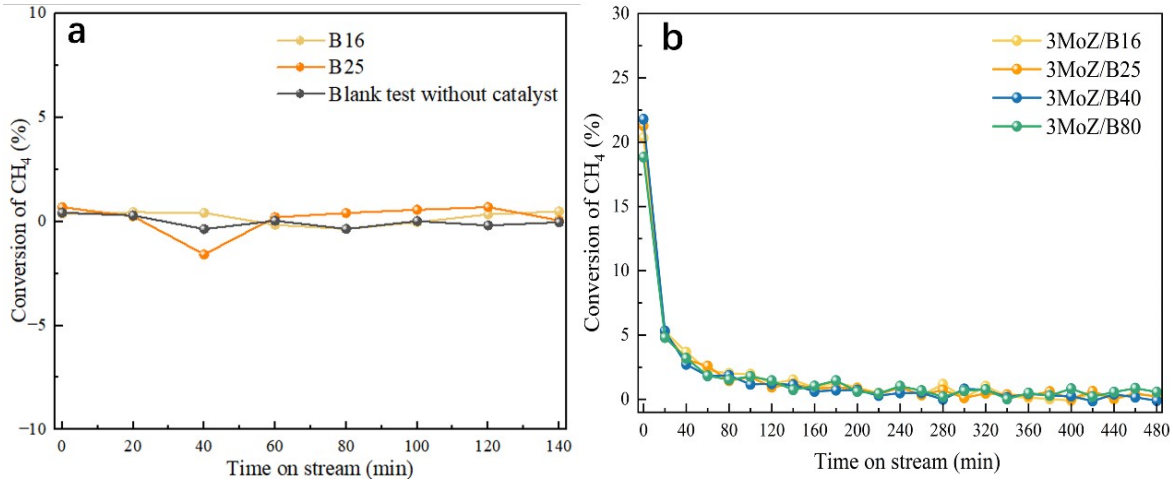

Figure S3 Blank test without catalyst and single-layer catalytic conversion rate of deboronation catalyst（a）and 3MoZ/BX double-layer catalyst methane conversion rate（b）

The MDA experiment conducted in an empty reactor showed a methane conversion rate of only 0.2% after calculation, indicating that the experimental error of the catalytic system can be neglected. Similarly, the conversion rate of the single-layer MDA catalytic conversion reaction of the weakly acidic Bsn-S-X series was also approximately zero, indicating that the boron-depleted silica-rich catalyst lacks the ability to initiate the reaction.

4. IGMH analysis of different adsorption sites.

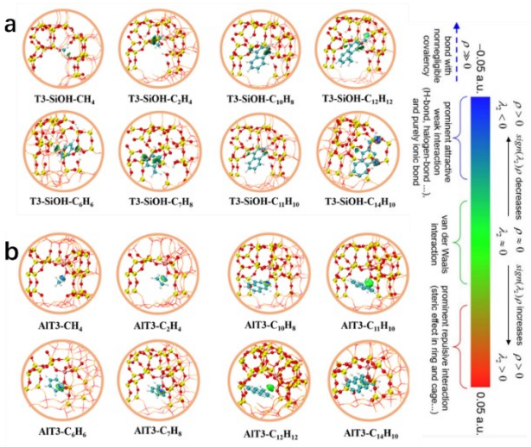

Figure S4 IGMH analysis of coke precursors adsorbed at vicinal silanols（a）and Al sites（b）

The interaction between coke deposit precursors and silanol structures is visualized using the IGMH method. The bluer the color of the interaction interface, the stronger the interaction, while green represents van der Waals forces and red indicates significant repulsive forces. The IGMH analysis of the adjacent silanol structures constructed by removing more Si atoms is shown in Figure S4a, which illustrates that the molecular sieve contains multiple pairs of adjacent silanol groups (T3-SiOH-) with weak hydrogen bonding interactions. From the color distribution of the adsorption interface, it can be observed that the adjacent silanol groups exhibit distinct blue regions when adsorbing carbon deposition precursors such as ethylene, dimethylnaphthalene, and anthracene, corresponding to their relatively high adsorption energies of 423.57 kJ/mol, 373.40 kJ/mol, and 372.43 kJ/mol, respectively. This indicates that the internal silanol structures exhibit high adsorption energies for all large-molecule carbon deposit precursors.

Compared to the weakly acidic silanol sites, the adsorption energies of benzene and toluene, the target products, at the Al sites reach 631.98 kJ/mol and 402.34 kJ/mol, respectively, demonstrating a significant advantage. As shown in Figure S4b, when methane, benzene, and toluene are adsorbed on Al sites, the region between the carbon atoms of the coke deposit precursors and the hydrogen atoms in the Al-O-H bonds appears as a distinct dark blue, indicating that they are bound through strong hydrogen bonding. However, the adsorption energies of ethylene and naphthalene at Al sites are lower than those at silanol nests and adjacent silanol sites, indicating that Al sites exhibit stronger adsorption capacity for small-molecule carbon deposit precursors than for large-molecule carbon deposit precursors. This suggests that, in the presence of these active sites, ethylene and naphthalene are more likely to adsorb onto internal silanol defects and undergo further dehydrogenation to form coke. In contrast, benzene and toluene are more likely to adsorb onto Al sites and form coke.

5. morphological characterization of the catalyst

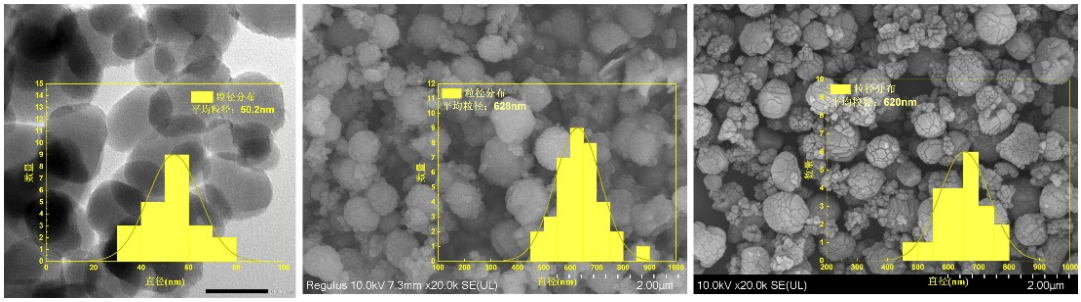

Figure S5 morphological characterization of the catalyst and its particle size distribution (samples from left to right are B25, EB25, and AB25)

6. Changes in methane conversion rates over time for B25 series catalysts

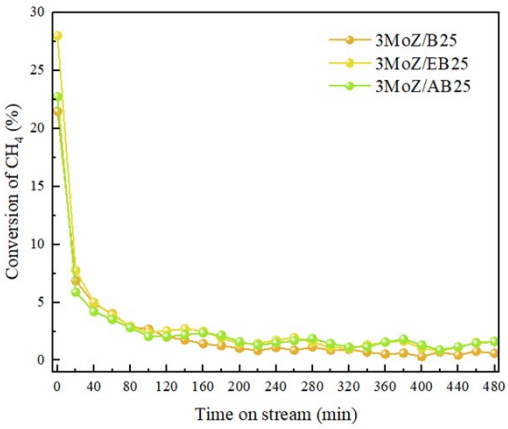

Figure S6 MDA conversion rate of B25 series catalysts

7. N_2 adsorption-desorption and BET data of commercial catalyst samples before and after treatment、Mo loading, and spent catalysts

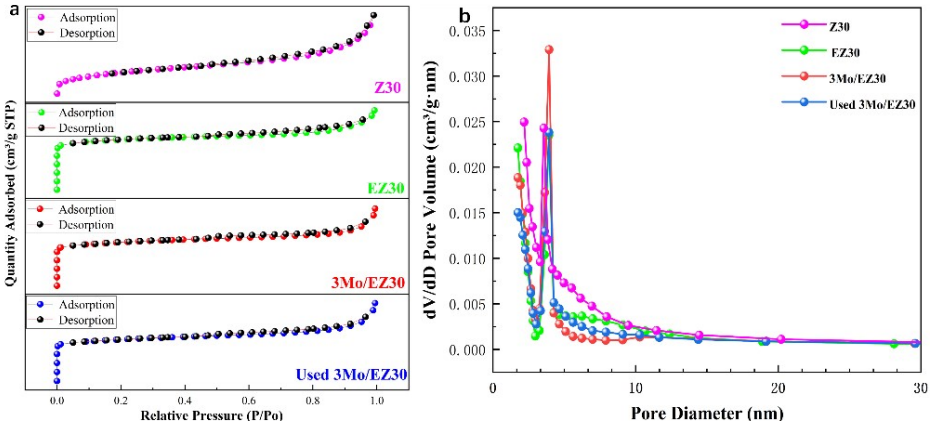

Figure S7 N_2 adsorption-desorption curves (a) and pore size distribution (b) of the commercial catalyst series

8. Methane conversion rate before and after EDA treatment with commercial catalyst

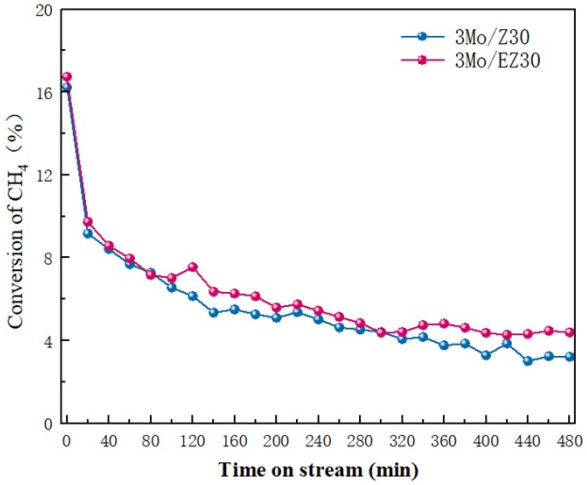

Figure S8 Sample catalytic performance in 700 °C MDA (a)

9. TEM image of commercial catalyst after 8 hours of reaction

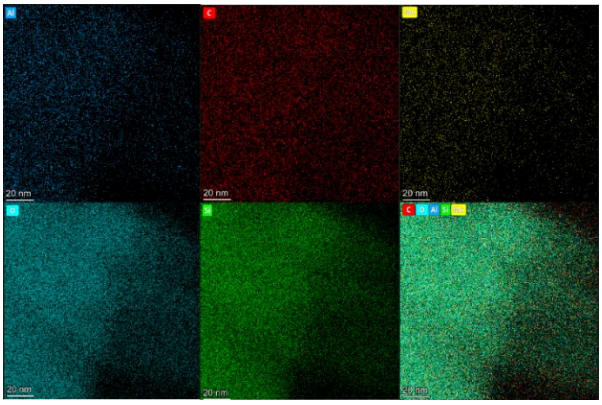

Figure S9 Mapping of the spent 3Mo/Z30catalyst after MDA for 8h

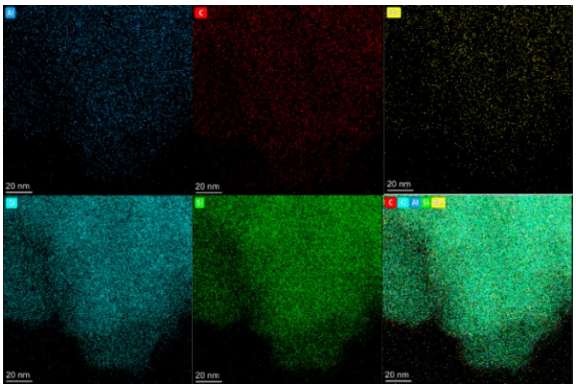

Figure S10 Mapping of the spent 3Mo/EZ30catalyst after MDA for 8h

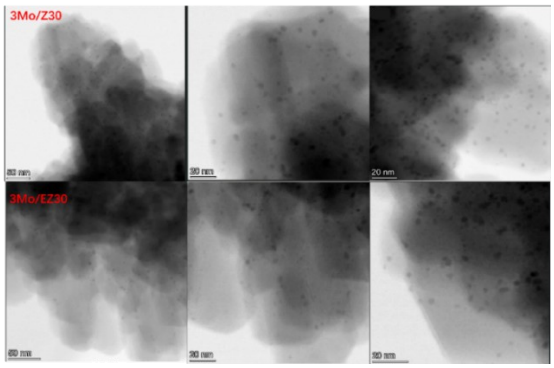

Figure S11 TEM images of 3Mo/Z30 and 3Mo/EZ30 after reaction

10. Statistics on specific surface area and pore volume of EB25 and AB25

Table S1 BET data for EB25 and AB25 catalysts

	Surface area (m^2 g^{-1})	Pore volume (cm^3 g^{-1})		
Samples	S_{total}[a]	V_{total}[b]	V_{micro}[b]	V_{meso}[b]
B25	312	0.46	0.03	0.43
EB25	357	0.52	0.12	0.40
AB25	371	0.65	0.08	0.57

a S_{BET} (specific surface area) is calculated by BET method.

b V_{micro}(microporous volume) and V_{meso}(mesoporous volume)are calculated by BJH method.

11. Comparison of this study with other studies on the performance of anti-coking strategies

Table S2 Detailed information on anti-coking strategies in the literature

Catalyst	Reaction time(h)	Temperature(℃)	GSHV(ml/g_{cat}·h)	Anti-coke deposit strategy	Mode of treatment	Changes in coke yield(mg/g)		Changes in aromatics yield(mg/g)		Coke reduction(%)	Aromatics increase (%)	Ref.
						before modification	after modification	before modification	after modification			
Mo/ZSM-5	15	700	1500	Enhance dispersion	Load Mo under supercritical thermal conditions	51.2	46	103	140.23	10.15	36	69
Mo/ZSM-5	12	700	1710	Passivation acid sites	salinization of the outer surface	130	100	—	—	23.07	20	70
Mo/ZSM-5	8	700	1500		Metal cation modification	18.7	4.1	153.15	160.87	40+	5.04	71
Mo/ZSM-5	24	700	1500		Al $(NO_3)_3$ solution treatment	37.8	33.6	51.3	96	29	11.1	72
Mo/ZSM-5	24+	700	2700		APTES treatment	18.3	12.3	49.5	66.2	32.7	5.97	73
Fe/ZSM-5	6	750	30000		Bimetallic Fe/Mg	128.8	120.3	155	156.58	6.60	1	74
					Bimetallic Fe/Ca	128.8	84.1	155	158.76	34.7	2.4	
Mo/S-1-ZSM-5	6.6	700	1500		H-ZSM-5 encloses the core-shell S-1 structure	66	48	81.9	109.2	27.30	33	75
Mo-Fe/ZSM-5	10	700	1500	Add iron additives	Impregnate a small amount of iron	69.3	55.6	41	57.4	19	40	76
Mo/ZSM-5	8	700	1560		EDA treatment	66.6	54.2	169.57	205.61	18.6	21.3	This work
								187.3	246.9		32.2	